Influence of interfaces on the perpendicular magnetic anisotropy in Tb/Fe multilayers

W.-S. Kim, W. Andrä,* and W. Kleemann
Laboratorium für Angewandte Physik, Gerhard-Mercator-Universität Duisburg, D-47048 Duisburg, Germany
(Received 17 February 1998)

The influence of interfaces on the perpendicular magnetic anisotropy (PMA) in evaporated Tb/bcc-Fe multilayers with and without diamagnetic Y blocking layers, $\{Tb/Fe/Y\}_{10}$ [=Y(1), Fe-on-Tb], $\{Y/Fe/Tb\}_{10}$ [=Y(2), Tb-on-Fe] and $\{Tb/Fe\}_{10}$ [=Y(3)], is investigated using torque magnetometry as a function of the angle α between the applied field **H** and the film plane at temperatures $15\ K \leqslant T \leqslant 300\ K$. Interface-induced PMA becomes noticeable below the ordering temperatures of the TbFe alloy in the rough Tb/Fe interfaces of Y(1) ($T_C \geqslant 300$ K) and that of Tb at the smooth Tb/Fe interfaces of Y(2) ($T_C = 219$ K). The latter mechanism dominates at low T, as explained within the framework of a coupled layer model, which is also able to describe the magnetic cone states found in Y(1), Y(2), and Y(3) at $T < 100$ K. In Y(3) the PMA is significantly enhanced by interlayer coupling, leading to polar cone angles as small as 30°. [S0163-1829(98)07833-3]

I. INTRODUCTION

Since the discovery of perpendicular magnetic anisotropy (PMA) in rare-earth/transition metal multilayers,[1] they have intensively been studied. Apart from their unbroken high technological potential as magneto-optic recording media,[2] they attract scientific interest, e.g., in view of the origin of the PMA. Numerous different sources for the PMA have been proposed, e.g., dipolar interaction[3] and local structural anisotropy.[4] Sato[5] suggested that the PMA is attributed to an anisotropic distribution of Tb-Fe pairs aligned perpendicular to the film plane. Shan *et al.*[6] developed a model involving single-ion anisotropy for compositionally modulated films. This model is based on the formation of amorphous alloy at the interfaces and has been extended by Wang *et al.*[7] They calculated the temperature (T) dependence of the orientation of the averaged magnetic moment of bcc-Fe (α-Fe) using local crystal-field effects and strong antiferromagnetic coupling between Fe and Tb.

Recently, *in situ* Mössbauer spectroscopy on bilayers of Tb-on-Fe (top interface) and Fe-on-Tb (bottom interface) layers revealed that primarily the top interface induces the PMA of α-Fe at low T.[8] As a consequence of the different atomic radii and surface energies of Tb and Fe, respectively, different structures of top and bottom interfaces are expected. They give rise to an asymmetry in a Tb/Fe/Tb trilayer as studied by means of *in situ* resistance measurements.[9] Mössbauer studies on probe layers of ^{57}Fe showed that the top interfaces are sharp and crystalline (α-Fe), whereas the bottom interfaces are rough and amorphous.[10] Consequently, in the case of multilayers, the structures of the interfaces between the individual layers can be expected to play a predominant role. In a previous investigation[11] we have evidenced that the top and bottom interfaces contribute differently to the magnetization reversal using magneto-optic Kerr spectroscopy on Tb/Fe multilayers containing diamagnetic Ag blocking layers.[11] In this paper we report on the different influences of top and bottom Tb/Fe interfaces on the PMA and the magnetization reversal using torque magnetometry.

II. EXPERIMENTAL PROCEDURE

All samples, $\{Tb/Fe/Y\}_{10}$ [=Y(1): Fe-on-Tb interfaces], $\{Y/Fe/Tb\}_{10}$ [=Y(2): Tb-on-Fe interfaces], and $\{Tb/Fe\}_{10}$ [=Y(3)], are thermally evaporated on Si(111) substrates at room temperature (RT) in an ultrahigh vacuum system. The pressure is better than 2×10^{-9} mbar during evaporation. The deposition rates and film thicknesses are controlled by calibrated quartz microbalances located close to the substrate position. The deposition rates amount to 0.05 nm/s for Fe, Tb, and Y. The thicknesses of the individual layers are 5.0, 1.4, and 1.2 nm for Fe, Tb, and Y, respectively. According to wide-angle x-ray diffraction the layers are polycrystalline without any in-plane texture.

Additional structural properties of our samples have been obtained by Mössbauer spectroscopy.[12] Apart from a dominating crystalline α-Fe component sizeable contributions due to amorphous iron are identified. According to Mössbauer experiments on Tb/Fe multilayers with similar thicknesses of the Fe layers, $t_{Fe} = 3.8$ nm,[13] using ^{57}Fe probe layers with thickness $t(^{57}Fe) = 0.5$ nm, the amorphous Fe component is primarily concentrated at the interfaces. In agreement with the preceding experiments on Tb/Fe bilayers[8] different structures of the interfaces are encountered. Approximately 83 and 62 % of the corresponding spectral areas are found to refer to amorphous Fe at the bottom (Fe-on-Tb) and top (Tb-on-Fe) interfaces, respectively. Similar structural conditions are expected to be met at the Y/Fe interfaces in view of the chemical similarity of Y and Tb and in accordance with previous investigations of Y/Fe/Y triple layers.[14]

Torque curves (TC's) are obtained by means of torque magnetometry in a temperature range of $15\ K \leqslant T \leqslant$ RT as a function of the angle α between the applied field **H** and an arbitrary direction **e** within the film plane with an applied field of 720 kA/m (Fig. 1). The film plane is oriented perpendicularly to the plane of field rotation. The torque τ lies perpendicularly to the both the field **H** and the film normal $\tilde{\mathbf{n}}$ and is measured in a noncompensation mode while sweeping the applied field at intervals of $\Delta\alpha = 2°$ from $\alpha = 0°$ to 360° and back from $\alpha = 360°$ to 0° (counter-clockwise and clockwise, respectively; see Fig. 1).

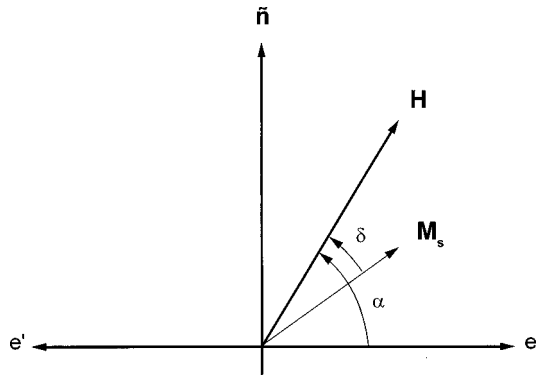

FIG. 1. Geometry of the torque measurements, where **H** is the applied field, $\mathbf{M}_S$ is the spontaneous magnetization, $\tilde{\mathbf{n}}$ is the film normal, $\alpha = \sphericalangle(\mathbf{e},\mathbf{H})$, $\delta = \sphericalangle(\mathbf{M}_S,\mathbf{H})$, and $\mathbf{ee}'$ is the cross section of the film plane perpendicular to the field-rotation plane containing **H** and $\tilde{\mathbf{n}}$.

III. RESULTS AND DISCUSSION

Figures 2 and 3 show the measured TC's of Y(1) and Y(2) at different temperatures, $15\,\mathrm{K} \leqslant T \leqslant 300\,\mathrm{K}$, respectively. At first glance both samples behave similarly with respect to the overall angular dependence and to its change with decreasing temperature. At $T \geqslant 200\,\mathrm{K}$ the observed TC's are typical of a sample with in-plane anisotropy.[15] An increasing torque τ is exerted to the film when rotating **H** out of the film plane. The sign of τ is defined by the sense of rotation, counterclock (CCW) or clockwise (CW). $|\tau|$ maximizes to a value $\tau_{\max}$ as $\alpha \to 90°$ and sawtoothlike changes sign at $\alpha > 90°$ owing to the flip of the in-plane component of $\mathbf{M}_S$ from **e** to **e**′ (Fig. 1).

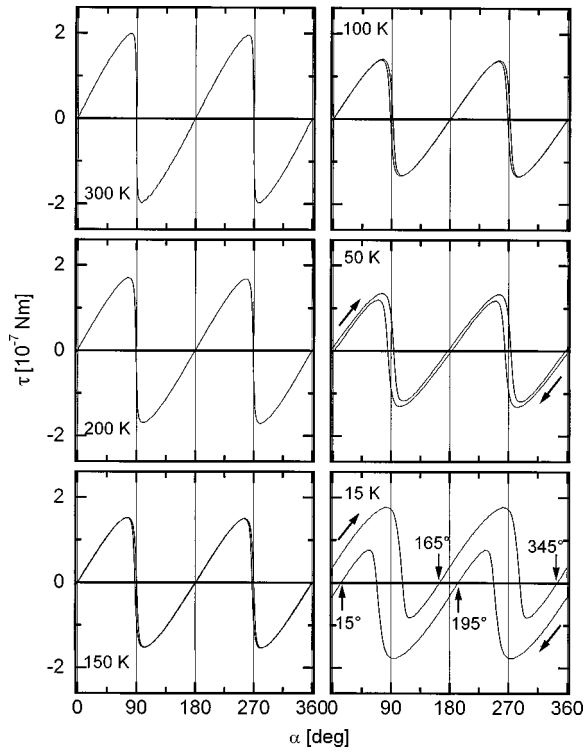

FIG. 2. Torque curves of Y(1) at different temperatures, $15\,\mathrm{K} \leqslant T \leqslant 300\,\mathrm{K}$, obtained with $H = 0.72$ MA/m. The film plane lies perpendicularly to the plane of field rotation. Arrows indicate the directions of the field rotation ($T = 15$ and 50 K) and the effective cone angles ($T = 15$ K, see text).

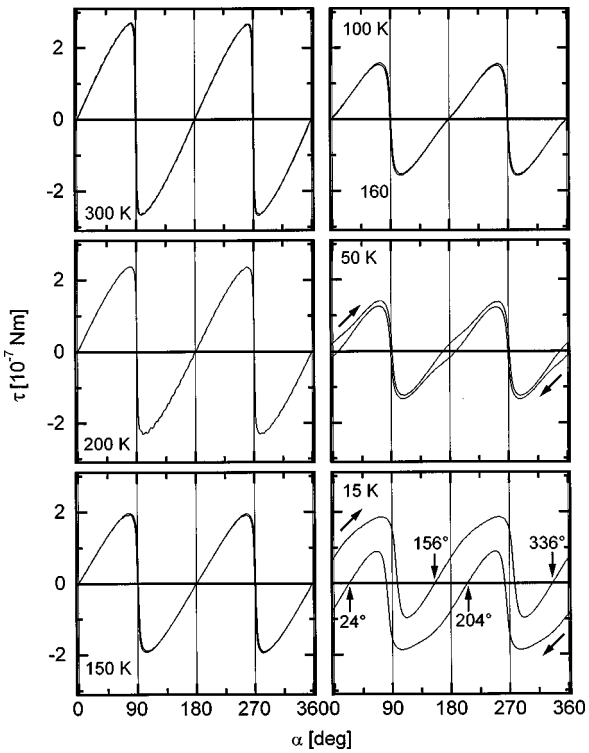

FIG. 3. Torque curves of Y(2) at different temperatures, $15\,\mathrm{K} \leqslant T \leqslant 300\,\mathrm{K}$, obtained with $H = 0.72$ MA/m. The film plane lies perpendicularly to the plane of field rotation. Arrows indicate the directions of the field rotation ($T = 15$ and 50 K) and the effective cone angles ($T = 15$ K, see text).

With decreasing temperature the amplitude of τ decreases. This behavior is attributed to a decrease of the in-plane anisotropy, or, in other words, to an increase of the PMA. A model calculation will be presented in Sec. IV. Here we remark that the decrease of $\tau_{\max}$ observed within the interval $0° < \alpha < 90°$ between $T = 300$ and 100 K, $\Delta\tau = \{\tau_{\max}(300\,\mathrm{K}) - \tau_{\max}(100\,\mathrm{K})\}/\tau_{\max}(300\,\mathrm{K})$, is about 20% larger in Y(2) ($\Delta\tau = 0.4$) than in Y(1) ($\Delta\tau = 0.32$). This indicates that the smooth Tb-on-Fe interfaces develop significantly larger PMA than the rough Fe-on-Tb interfaces when cooling to below the Curie temperature of crystalline Tb, $T_C(\mathrm{Tb}) = 219.3$ K.[16]

The TC's of Y(1) (Fig. 2) show not only a decrease of τ but also rotational hysteresis (RH) near $\alpha = 90°$ and 270° upon cooling to $T = 100$ K. Such a RH is, in terms of a coherent rotation model,[17] unexpected for an easy-plane system (see Sec. IV). Probably secondary intraplanar anisotropy or some kind of in-plane coercivity is encountered with decreasing T. It gives rise to domain pinning during magnetization reversal. Presumably this is due to the in-plane counterparts of the randomly distributed local anisotropy axes within the amorphous TbFe alloys[18] contained in the rough Fe-on-Tb interfaces. Remarkably, RH of this kind is much weaker in Y(2) (Fig. 3) owing to reduced alloying in the smooth Tb-on-Fe interfaces.

A closer look at the TC of Y(2) reveals a decrease of the slope in the vicinity of $\alpha = 0°$, 180°, 360°,... upon cooling to $T = 100$ K (Fig. 3). This is a first hint at magnetic heteroge-

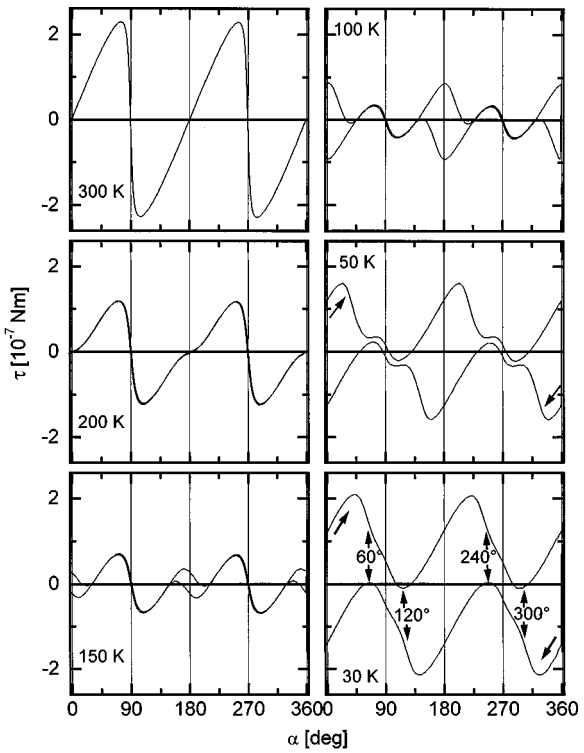

FIG. 4. Torque curves of Y(3) at different temperatures, 30 K$\leqslant T\leqslant$300 K, obtained with $H=0.72$ MA/m. The film plane lies perpendicularly to the plane of field rotation. Arrows indicate the directions of the field rotation ($T=30$ and 50 K) and the effective cone angles ($T=30$ K, see text).

neity to be considered within the bilayers. As will be shown in Sec. IV within an uncoupled two-layer model the S shape of the TC in the vicinity of, e.g., $\alpha=180°$ can be understood as a superposition of two TC's with opposite character. In addition to the dominant TC of in-plane magnetized bulk α-Fe a weak TC, opposite in sign and phase shifted by 90°, has to be considered. It is due to the Tb/Fe interfaces, which gain increasingly PMA as T is lowered to below T_C(Tb).

In the low-T region, $T\leqslant 50$ K, the RH of the two samples, Y(1) and Y(2), is no longer restricted to the vicinity of α=90°, 270°,..., but extends over the entire angular range, $0°\leqslant\alpha\leqslant 360°$ (Figs. 2 and 3). The curves for CCW and CW rotation of **H** are substantially shifted against one another. Similar, albeit uncommented effects were found by Krishnan *et al.*[19] on amorphous FeTb alloys at low temperatures. Owing to the well-known ferrimagnetic coupling between Tb and Fe spins[20] conical spin ordering takes place, where the Fe spins are preferentially aligned under intermediate polar angles, $0°<\theta_1<90°$.[21] Hence, zero mechanical torque should be observed whenever the field is parallel to the oblique easy direction, $\alpha\approx 90°\pm\theta_1$. This can be explained within the framework of an effective one-layer model exhibiting conical spin structure as discussed in Sec. V.

Figure 4 shows the TC's of the multilayer Y(3), which lacks any blocking layers of Y. It reveals similar temperature dependences as found in the case of Y(2). The angular regions around $\alpha=0°$ and 180° are characterized first by reduced slopes at $T=200$ K and then by the onset of RH at $T\leqslant 150$ K. These features appear at temperatures being about 100 K higher than for the corresponding situations observed on Y(2) (Fig. 3). In addition, the torque peaks in the vicinity of $\alpha=90°$ and 270° become drastically reduced at $T<150$ K. When comparing the torque amplitudes near 90° and 180°, obviously the contribution of PMA dominates at $T\leqslant 100$ K. This behavior strongly hints at mutual coupling of all interfaces, top and bottom, by virtue of the magnetized Tb layers. In addition, enhanced PMA within the α-Fe layers is expected owing to dipolar coupling between adjacent bilayers.[22] Strong PMA occurring in Tb/Fe multilayers without blocking layers is a well-known low-T feature as confirmed, e.g., by measurements of hysteresis cycles with magneto-optic Kerr effect and superconducting quantum interference device techniques.[23]

Peculiarly, however, upon further cooling to $T=30$ K the TC does not become symmetric around the normal directions, $\alpha=90°$ and 270°. We observe sawtoothlike curves, the zeros of which are shifted by about $\pm 30°$ with respect to the expected positions. Again, conical spin structure has to be taken into account. Details within an effective one-layer model will be presented in Sec. V.

IV. UNCOUPLED TWO-LAYER MODEL

The TC's observed on Y(1), Y(2), and Y(3) ($T>100$ K) can be modeled by a computer simulation based on a two-layer model involving two different anisotropies, in-plane in the bulk α-Fe and out-of-plane in the interfaces between Fe and Tb layers, respectively. The magnetization reversal process is described by the Stoner-Wohlfarth (SW) coherent rotation model[17] assuming homogeneous magnetization within each layer. The free energy of the two-layer system in an applied field **H**, involving first-order uniaxial anisotropies and interlayer coupling, reads

$$E=\sum_{i=A,B} V_i K^i_{\rm eff}\sin^2(\alpha-\delta_i) - \sum_{i=A,B}\mu_0 V_i M^i_S H\cos\delta_i - \Lambda^* S M^A_S M^B_S\cos(\delta_A-\delta_B). \quad (1)$$

V_i and M^i_S are the volumes and the saturation magnetizations of the layers $i=A$ and B, respectively. By definition layer A consists of bulk Fe, whereas layer B includes both bulk Tb and the adjacent ferrimagnetically coupled monolayers of Fe, δ_i and α represent the angles between $\mathbf{M}^i_S$ and **H**, and **H** and **e**, respectively (Fig. 1). The anisotropy constants $K^i_{\rm eff}$ account for both the uniaxial anisotropy constants K^i_u and the shape anisotropy $\mu_0/2(N_\perp-N_\parallel)M^2_S$, where μ_0, $N_\perp$, and $N_\parallel$ are permeability of vacuum, the demagnetizing factors perpendicular and parallel to the film plane, respectively. In the following we shall assume $K^A_{\rm eff}>0$ and $K^B_{\rm eff}<0$, i.e., effective planar and perpendicular anisotropy energy densities of the layers A and B, respectively. Λ^* describes the exchange coupling between the Fe atoms at the interface (area S) and the α-Fe in the bulk. Its sign depends on the magnitude of the Tb moments in layer B and may switch from positive to negative upon lowering the temperature. Below we shall consider the limiting cases of weak ($M_B\approx 0$) and strong coupling

($M_B \neq 0$), which seem approximately to apply to the cases of negligible ($T > 200$ K) and fully active interlayer coupling at $T \leqslant 50$ K.

Minimization of E with respect to the angles δ_i leads to the equilibrium positions of the magnetization vectors. Necessary conditions are

$$\frac{\partial E}{\partial \delta_A} = -k_A \sin 2(\alpha - \delta_A) + \mu_0 m_A H \sin \delta_A + \Lambda m_A m_B \sin(\delta_A - \delta_B) = 0 \tag{2}$$

and

$$\frac{\partial E}{\partial \delta_B} = -k_B \sin 2(\alpha - \delta_B) + \mu_0 m_B H \sin \delta_B - \Lambda m_A m_B \sin(\delta_A - \delta_B) = 0, \tag{3}$$

where the magnetic moments $m_A = V_A M_S^A$, $m_B = V_B M_S^B$, the anisotropy energies $k_A = V_A K_{\text{eff}}^A$, $k_B = V_B K_{\text{eff}}^B$ and the coupling constant $\Lambda = \Lambda^* S / V_A V_B$ are introduced. The torques τ_i of layer $i = A$ and B exerted by the external field H are given by

$$\tau_A = \mu_0 m_A H \sin \delta_A = -\Lambda m_A m_B \sin(\delta_A - \delta_B) + k_A \sin 2(\alpha - \delta_A) \tag{4}$$

and

$$\tau_B = \mu_0 m_B H \sin \delta_B = \Lambda m_A m_B \sin(\delta_A - \delta_B) + k_B \sin 2(\alpha - \delta_B). \tag{5}$$

Let us first assume weak interlayer coupling, $\Lambda = 0$. Then by using the Eqs. (4) and (5) the normalized torques may be written as

$$T_{A,B} = \frac{\tau_{A,B}}{k_{A,B}} = h_{A,B} \sin \delta_{A,B} = \sin 2(\alpha - \delta_{A,B}), \tag{6}$$

where $h_{A,B} = \mu_0 m_{A,B} H / k_{A,B}$.

Solving the right-hand sides of Eq. (6) independently for δ_A and δ_B one may calculate $T_{A,B}$ vs α numerically. Figure 5 shows the calculated TC's for the individual layers A (a) and B (b) at various reduced fields, $0.3 \leqslant |h_{A,B}| \leqslant 2$, where $h_A > 0$ and $h_B < 0$ account for the different anisotropies involved. The shapes of the TC's are similar for both anisotropies except for a mutual shift by 90° and the lack of RH in the easy-plane case [Fig. 5(a)]. Moreover, the easy-plane case does not show the transition to a $\sin \alpha$ behavior for $h_A < 0.5$. In the extreme cases of weak and strong relative anisotropy, $|h_{A,B}| > 1$ and < 0.5, the well-known sawtooth and sinusoidal TC's for easy-axis anisotropy, respectively, are obtained. The system with out-of-plane anisotropy shows irreversible torque behavior around $\alpha = 0°$ and 180° [Fig. 5(b)]. In the following we shall try to model the measured TC's by best fitting to linear combinations with appropriate amplitudes A, B, and relative fields, $h_{A,B}$.

Figure 6(a) shows the results for the TC obtained on Y(3) at $T = 200$ K (Fig. 4), which is best fitted by the function $\tau(\alpha)/10^{-7}$ Nm $= 2.65 \times T_A(h_A = 1.3) + 0.55 \times T_B(|h_B| = 2)$, where T_A $(= \tau_A / k_A)$ and T_B $(= \tau_B / |k_B|)$ are normalized

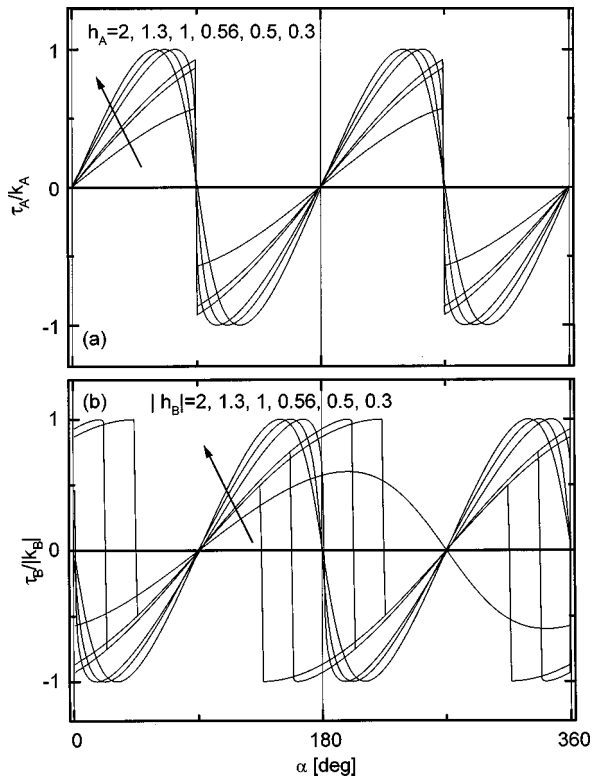

FIG. 5. (a) Normalized torque curves τ_A / k_A for easy plane oriented parallel to the film plane calculated for different values of $h = H/H_K$. (b) Normalized torque curves $\tau_A / |k_B|$ for easy axis oriented perpendicular to the film plane calculated for different values of $|h| = H/H_K$.

TC's as presented in Fig. 5. Obviously two slightly distorted $\sin 2\alpha$-like functions with different sign are superimposed, both of which indicate weak relative anisotropies. The dominating contribution is due to the in-plane anisotropic bulk α-Fe sublayers. Nevertheless, the counteracting contributions due to the PMA of the interfaces are noticeable. They give rise to flattening of $\tau(\alpha)$ in the vicinity of $\alpha \approx 0°$ and 180°. In a similar way the TC's of Y(1) (Fig. 2) and Y(2) (Fig. 3) observed at $T \geqslant 100$ K may be modeled with nonhysteretic $T_{A,B}$ curves (Fig. 5) in the weak anisotropy limit.

Evaluation of the fitting parameters emerging from Fig. 6(a), $h_A = 1.30$ and $\tau_A / k_A = 2.65$, yields $M_A = 1.14$ MA/m and $K_{\text{eff}} = 7.89 \times 10^5$ J/m^3. In these figures layer A refers to α-Fe films, whose thickness $t_A = 4.25$ nm takes into account that three atomic Fe layers of thickness 0.75 nm are mixed into layer B.[8] M_A amounts to only about 2/3 of the bulk α-Fe value, $M_{\text{Fe}} = 1.7$ MA/m, although the value of the hyperfine field, $B_{\text{HF}} = 34$ T, hints at normal crystalline environment.[12] Very probably this discrepancy is due to the spin canting, which yields $\langle \theta \rangle = 44°$ in the α-Fe films.[12] Hence, only the planar component of the magnetization, $M_A = M_S \sin\langle \theta \rangle = 1.18$ MA/m, contributes to τ_A, whereas the perpendicular components seem to cancel each other. Spin canting due to induced PMA is also the reason for the small value of K_{eff}. It falls below the shape anisotropy, $(\mu_0/2) M_A^2 = 8.16 \times 10^5$ J/m^3, by an amount of $K_U = 0.27 \times 10^5$ J/m^3.

The TC measured on Y(3) at $T = 100$ K is best fitted by the function $\tau/10^{-7}$ Nm $= 1.05 \times T_A(h_A = 1.3) + 1.4 \times T_B(|h_B| = 0.56)$ as shown in Fig. 6(b). The fit is satisfying

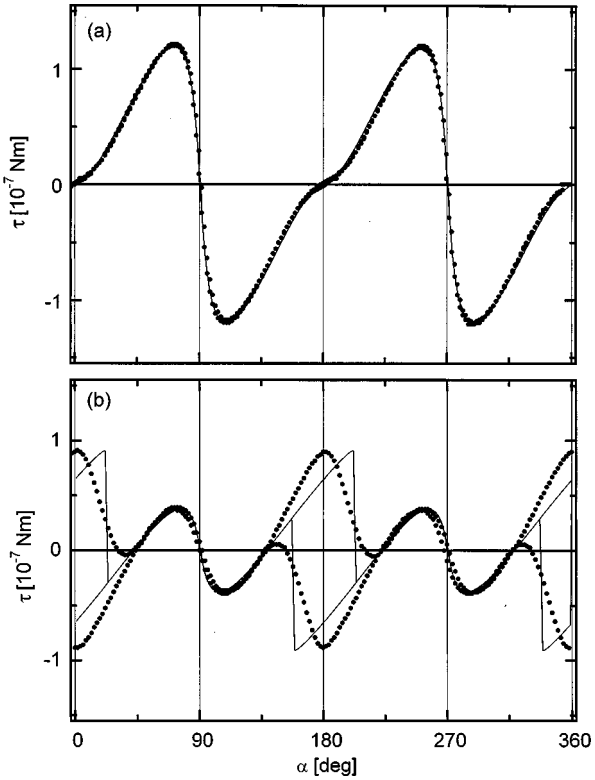

FIG. 6. Comparison of calculated (solid lines) with measured torque curves (solid circles) obtained on Y(3) at $T=200$ (a) and 100 K (b) (cf. Fig. 4; see text).

except in the vicinity of $\alpha=0°$ and 180°, where RH occurs. Whereas the experimental data are smoothly varying, the calculated curves reveal abrupt jumps of τ at certain switching angles. These are in fact expected within the framework of the SW model, which anticipates homogeneous magnetization, coherent spin rotation and sharp first-order jumps. Experimentally, however, these discontinuities seem to be smeared out by nucleation and multidomain processes. Anticipating the discussion of Sec. V we remark that part of the observed rounding has also to do with switching on a cone rather than collinear spin states as presumed in our simple two-layer model. As compared with the TC observed at $T=200$ K [Fig. 6(a)] the relative amplitude of the A component, $k_A/(k_A+k_B)$, with planar anisotropy decreases from 83 to 43%. In parallel, the contribution due to the perpendicularly anisotropic B component, $k_B/(k_A+k_B)$, rises from 17 to 57%. Simultaneously it corresponds to a relatively large anisotropy constant as reflected by the weak relative field, $|h_B|=0.56$. That is why hysteresis becomes noticeable at $T<200$ K in the $\alpha=0°$ and 180° regions (Fig. 4).

Similar albeit much weaker splitting is observed in Y(2) (Fig. 3) in the same angular regions, $\alpha=0°$ and 180°, but at lower temperatures, $T\leqslant 50$ K. Since such a looplike phenomenon is absent in Y(1) (Fig. 2), we are inclined to attribute larger tendency towards PMA to Tb/Fe layer systems containing smooth Tb-on-Fe interfaces. This is corroborated by another signature indicating increasing contributions of PMA with decreasing temperature. When cooling Y(1), Y(2), and Y(3) from $T=300$ to 100 K, say (Figs. 2–4) we observe significant decreases of the sawtooth peak height at $\alpha\approx 90°$. Within the two-layer model this phenomenon can be explained by growing B-type contributions with inverted sign [Fig. 5(b)], which eventually may become hysteretic as $|h_B|$ becomes smaller than unity at low T [Y(2) and Y(3), see above].

V. CONE STATE MODEL

In the low-T regions, $T\leqslant 50$ K, the hysteresis starts to spread over the whole angular range, $0°\leqslant\alpha\leqslant 360°$, in all samples, Y(1), Y(2), and Y(3) (Figs. 2–4). This phenomenon cannot be explained within the uncoupled two-layer model, Eq. (6), where the hysteresis loops are expected to be localized around certain angles, $\alpha=0°$, 90°, 180°, etc. Contrastingly, we find sawtoothlike TC's, where the CCW and the CW counterparts are shifted against one another along both the α and the τ axes. This feature appears most pronounced at very low temperatures, $T=15-30$ K. For its explanation we consider the following conjectures: (i) strong magnetic coupling within bulk and interface sublayers invalidates the uncoupled two-layer model and reinstalls an effective one-layer model, (ii) strong ferrimagnetic coupling between Tb and Fe spins create sperimagnetic magnetization ordering with easy axes lying on cones under polar angles θ_1 and $\theta_2=180°-\theta_1$ with respect to the film normal. The latter property has frequently been verified on the Fe magnetization, $\mathbf{M}_A$, by using Mössbauer spectroscopy in both Tb/Fe alloys[21] and multilayers.[24] Recently, low-T angles $\theta_1\approx 30°-35°$ have been determined in samples being similar to the present ones with Y replaced by Ag blocking layers.[25]

In order to describe the observed spin canting let us assume strong PMA within the interface such that $\mathbf{m}_B$ is always orientated perpendicularly to the film plane, $\alpha-\delta_B=\pm\pi/2$. Equation (1) then reads

$$E=k_A\cos^2\theta_A+k_B-\mu_0 H[m_A\sin(\alpha+\theta_A)\pm m_B\sin\alpha]\mp\Lambda m_A m_B\cos\theta_A, \tag{7}$$

where $\theta_A=\pi/2+\delta_A-\alpha$ is the angle between $\mathbf{m}_A$ and $\tilde{\mathbf{n}}$ (Fig. 1). In zero external field, $H=0$, minimization of E with respect to θ_A yields the equilibrium canting angles

$$\theta_{1,2}=\cos^{-1}\left(\pm\frac{\Lambda m_A m_B}{2k_A}\right), \tag{8}$$

which define the cone states depicted by the orientations 2, 3 and 1, 4 in Fig. 7, where $\theta_1+\theta_2=\pi$.

It should be noticed that the solutions $\theta_A=0$ or π of $dE/d\theta_A=0$ refer to maxima of E provided that $|\Lambda|<2k_A/m_A m_B$. This is indeed, inferred from Mössbauer studies,[8,12] where intermediate canting angles, $0<\langle\theta_A\rangle<\pi/2$, have been reported for Tb/Fe multilayers even at lowest temperatures. On the other hand, however, strong coupling, viz. $|\Lambda|\geqslant 2k_A/m_A m_B$, seems to follow from the fact that $\langle\theta_A\rangle$ changes but weakly when applying perpendicular magnetic fields up to $H=4$ MA/m at low T.[12] Very probably, in addition to the canting mechanism described by Eq. (8), random local tilting of $\mathbf{m}_B$ out of the normal direction might cause similar tilting of $\mathbf{m}_A$ via strong coupling. The directional disorder in the Tb/Fe interfaces resembles that observed in sperimagnetic amorphous TbFe alloy systems due to random anisotropy mechanisms.[21] Thus being essentially

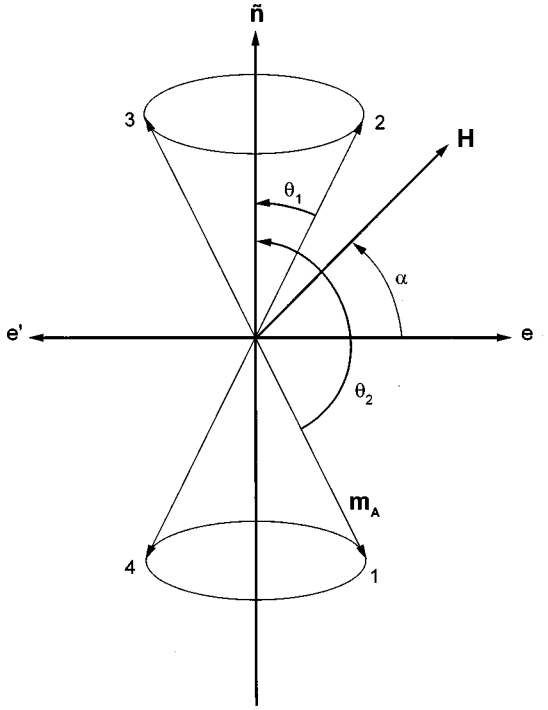

FIG. 7. Illustration of cone states referred to the measured TC of Y(3) at $T=30$ K (Fig. 4). θ_1 and θ_2 are the cone angles with respect to the film normal (see text).

in the strong-coupling limit it seems justified to neglect decoupling of $\mathbf{m}_A$ and $\mathbf{m}_B$ by our probing field, $H=0.72$ MA/m, and to assume $\theta_{1,2}$ to be constant while scanning a TC.

Equation (7) then yields

$$\tau(\alpha) = -\mu_0 H[m_A \cos(\alpha+\theta_A) \pm m_B \cos\,\alpha], \tag{9}$$

with $\theta_A = \pm\theta_{1,2}$ defined by Eq. (8). Vanishing torque, $\tau=0$, is expected for angular positions

$$\cos\,\alpha = \pm \frac{\sin\,\theta_{1,2}}{\sqrt{1+(m_B/m_A)^2+\Lambda m_B^2/k_A}}. \tag{10}$$

In the limit $\mathbf{m}_B \to 0$ one obtains $\cos\alpha \approx \pm\sin\theta_{1,2}$, which leads to four different angles, $\alpha = \pm\theta_1 \pm \pi/2$. Hence, $\tau(\alpha)$ should vanish, whenever α coincides with one of the easy cone directions 1–4 (Fig. 7), where single domains of $\mathbf{m}_A$ are collinear with **H**. This result approximately holds also at finite values of $\mathbf{m}_B$, in particular below the compensation temperature where the negative sign of Λ applies.

As can be seen in Fig. 4, however, this expectation is only partly met. Only two of the easy directions give rise to zero torque, $\tau \approx 0$, namely $\alpha = 270° + \theta_1$ (denoted as domain 1 in Fig. 7), $90° + \theta_1$ (domain 3) for the CCW and $\alpha = 90° - \theta_1$ (domain 2), $270° - \theta_1$ (domain 4) for the CW TC, where $\theta_1 \approx 30°$ in agreement with $\langle\theta\rangle$ data obtained on similar Tb/Fe multilayers.[25] At a closer look, however, the missing easy directions are indicated by slight dips in both TC's (vertical arrows in Fig. 4). Obviously, the large field limit (see above) is not met in our experiment. Instead of being single domain the sample attains a multidomain structure with varying weight of the four possible easy directions. Full switching from, say, the lower to the upper cone state takes place only when **H** attains its extreme normal component in the vicinity of $\alpha = 90°$. That is why full alignment of **M** is not realized at $\alpha = 90° - \theta_1$ (domain 2), but in domain 3 upon rotating **H** first to $\alpha = 90°$ and then into its easy direction, $\alpha = 90° + \theta_1$. The CCW curve in Fig. 4 is thus understood by hysteretic switching between the domains 1 and 3, where $\tau \geqslant 0$ at any angular position. The domains 2 and 4 are only partly populated at intermediate angles (see above). When changing the sense of scanning, the torque changes sign such that $\tau \leqslant 0$ at any value of α. In the CW curve, hence, switching takes place between the fully aligned domains 2 and 4, whereas 1 and 3 are only partly aligned when hitting their respective easy directions. The smoothness of the observed TC's clearly indicates absence of sharp switching processes. Very probably nucleation and domain growth take place on a microscopic scale. Hence, the total torque observed will be a weighted superposition of four $\tau(\alpha)$ curves according to Eq. (9), the micromagnetic model of which is presently not available.

The preceding discussion also provides some understanding of the peculiar mutual shifts between the CCW and CW TC's observed on Y(1) and Y(2) at $T<100$ K (Figs. 2 and 3). Obviously in these cases, again, cone states are realized in the bulk of their Fe layers. Assuming smaller values $|\Lambda m_B/m_A|$ than in the case of the strongly uniaxial Y(3) sample (Fig. 4), intraplanar anisotropy prevails in these cases. In the situation met, e.g., for Y(1) at $T=15$ K in Fig. 2 we assume $\theta_1 \approx 75°$. Upon rotating **H** in the CCW direction switching takes place preponderantly between the nearly planar domains 1 and 3 with $\tau(\alpha)=0$ at $\alpha = 90° + \theta_1$ and $270° + \theta_1$. Conversely the CW torque signal vanishes when hitting the easy directions 2 and 4 at $\alpha = 90° - \theta_1$ and $270° - \theta_1$. Owing to sufficiently large uniaxial anisotropy, $k_B > 0$, switching between domains 1 and 2 (3 and 4) is delayed. This explains the positive bias superimposed to the CCW TC, while it becomes negative when scanning into the CW direction. Remarkably, the largest angular hysteresis is found at $\alpha = 90°$ and 270° in all cases shown in Figs. 2 and 3. In the vicinity of these angles hysteresis survives even at temperatures as high as $T=150$ K in Y(1).

VI. CONCLUSIONS

Our investigations have shown that the two different Tb/Fe interfaces, rough [bottom, Fe-on-Tb, Y(1)] and smooth [top, Tb-on-Fe, Y(2)], respectively, induce PMA by different amounts. The appearance of hysteresis in the vicinity of $\alpha = 0°, 180°, 360°, \ldots$, in the TC's of Y(2) at $T<100$ K (Fig. 3) is the key issue indicating stronger PMA in Y(2) than in Y(1). This is readily understood within the framework of our cone state model. Equation (8) indicates decreasing PMA for increasing θ_1, hence, decreasing m_B, if Λ, m_A, and k_A are considered as constants. Indeed, in the case of rough interfaces encountered in Y(1), the Fe atoms are distributed in a relatively large volume of an amorphous TbFe alloy. Hence, only a small fraction of them exhibits direct exchange interaction with the adjacent α-Fe layer. This explains the fairly large low-T cone angle, $\theta_1 = 75°$, in Y(1) compared to those in Y(2), $\theta_1 = 66°$, or in Y(3), $\theta_1 \approx 30°$ (Figs. 2–4).

Contrastingly with these low-T observations the decrease

of τ_{max} between $T=300$ and 250 K is substantially larger in Y(1) (6%) than in Y(2) (2%). Hence, in this temperature range PMA evolves more effectively in Y(1) than in Y(2). Very probably this is a consequence of interface alloying. In Y(1) this enhances the ferrimagnetic ordering temperature compared to that of pure Tb, 219 K, above which PMA is virtually suppressed in Y(2). This is corroborated by evaluating TC's recorded at various fields, $480\ \mathrm{kA/m} \leqslant H \leqslant 720\ \mathrm{kA/m}$, at room temperature. Using the relationship for the inverse slope at $\alpha = 0°$ or 180° (Ref. 26)

$$\frac{d\alpha}{d\tau} = \frac{1}{\mu_0 V M_S H} + \frac{1}{2VK_{\mathrm{eff}}} + \frac{1}{D}, \tag{11}$$

where D is the torsion constant of the torsion fiber, we obtain $M_S = 956$, 985, 1012 kA/m and $K_U = K_{\mathrm{eff}} - (\mu_0/2)M_S^2 = 1.70$, 1.07, 2.51×10^5 J/m^3 for Y(1), Y(2), and Y(3), respectively. Here an effective single layer model is assumed and K_U refers primarily to the interface PMA. M_S, which refers to the total volume V of the multilayers, is virtually independent of their kind. In contrast, the K_U values differ considerably, being lowest in Y(2), intermediate in Y(1) (thanks to interface alloying), and largest in Y(3) (owing to additional coupling, see below). The observed canting angles, $\langle \theta \rangle = 79.1°$, 75.9°, 70.4° (Ref. 12) are in qualitative agreement with these assertions.

PMA due to coupling with both top and bottom interfaces is much more pronounced in Y(3) multilayers (Fig. 4). Large effects are already observed when cooling from RT to 200 K, probably due to the ferrimagnetic polarization in the rough bottom interfaces. Even more spectacular effects occur upon cooling further down to 30 K, where the smooth top layers are assumed to play a major role. In addition, the overall PMA becomes enhanced by dipolar coupling of the α-Fe layers via the intercalated magnetic Tb layers. A similar mechanism was proposed to be active in other rare-earth transition-metal multilayers like CeH_2/Fe.[3]

The relevance of two different modifications of Fe residing in the bulk and in the interfaces, respectively, has become manifest in our above model calculations. When considering either vanishing or strong coupling, respectively, features like hysteresis and magnetic cone states have been described semiquantitatively. The more laborious analysis of intermediate coupling, which certainly describes the experimental results more realistically, will be left for future studies.

ACKNOWLEDGMENTS

The authors are indebted to J. Tappert and W. Keune for discussions and providing the samples. This work was supported by the Deutsche Forschungsgemeinschaft through SFB 166.

*Also at Institut für Physikalische Hochtechnologie Jena, Helmholtzweg 4, D-07743 Jena, Germany.

[1] T. Morishita, Y. Togami, and K. Tsushima, J. Phys. Soc. Jpn. **54**, 37 (1985).
[2] M. Tanaka, H. Yuzurihara, and T. Tokita, IEEE Trans. Magn. **MAG-23**, 2955 (1987).
[3] O. Schulte, F. Klose, and W. Felsch, Phys. Rev. B **52**, 6480 (1995).
[4] Y. Fujiwara, X. Y. Yu, S. Tsunashima, S. Iwata, M. Sakurai, and K. Suzuki, J. Appl. Phys. **79**, 6270 (1996).
[5] N. Sato, J. Appl. Phys. **59**, 2514 (1986).
[6] Z. S. Shan, D. J. Sellmyer, S. S. Jaswal, Y. J. Wang, and J. X. Shen, Phys. Rev. B **42**, 10 446 (1990).
[7] Y. J. Wang, C. P. Luo, W. Kleemann, B. Scholz, R. A. Brand, and W. Keune, J. Appl. Phys. **73**, 6907 (1993).
[8] B. Scholz, R. A. Brand, and W. Keune, Phys. Rev. B **50**, 2537 (1994).
[9] C. Dufour, K. Cherifi, A. Bruson, G. Marchal, and Ph. Mangin, Phys. Status Solidi A **125**, 561 (1991).
[10] J. Tappert, J. Jungermann, B. Scholz, R. A. Brand, and W. Keune, J. Appl. Phys. **76**, 6293 (1994).
[11] W.-S. Kim, W. Kleemann, J. Tappert, and W. Keune (unpublished).
[12] J. Tappert *et al.* (unpublished).
[13] F. Richomme, B. Scholz, R. A. Brand, W. Keune, and J. Teillet, J. Magn. Magn. Mater. **156**, 195 (1996).
[14] S. Handschuh, J. Landes, U. Köbler, Ch. Sauer, G. Kisters, A. Fuss, and W. Zinn, J. Magn. Magn. Mater. **119**, 254 (1993).
[15] M. J. Pechan, M. E. Bait, and B. D. Paul, J. Appl. Phys. **69**, 5085 (1991).
[16] R. J. Elliot, *Magnetic Properties of Rare Earth Metals* (Plenum, London, 1972).
[17] E. C. Stoner and E. P. Wohlfarth, Proc. R. Soc. London, Ser. A **240**, 599 (1948).
[18] R. Alben, J. J. Becker, and M. C. Chi, J. Appl. Phys. **49**, 1653 (1978).
[19] R. Krishnan, M. Porte, M. Tessier, J. P. Vitton, and Y. Le Cars, IEEE Trans. Magn. **MAG-24**, 1773 (1988).
[20] I. A. Campbell, J. Phys. F **2**, L47 (1972).
[21] J. P. Eymery, A. Fnidiki, R. Krishnan, M. Tessier, and J. P. Vitton, Phys. Rev. B **38**, 11 931 (1988).
[22] A. Suna, J. Appl. Phys. **59**, 313 (1986).
[23] W.-S. Kim *et al.* (unpublished).
[24] B. Scholz, R. A. Brand, and W. Keune, J. Magn. Magn. Mater. **104-107**, 1889 (1992).
[25] O. Marks, T. Ruckert, J. Tappert, W. Keune, W.-S. Kim, W. Kleemann, and J. Voiron, IEEE Trans. Magn. (to be published).
[26] W. Andrä, Phys. Status Solidi **1**, K135 (1961).